Rock and Soil Mechanics 2025 46(12): 3740−3756 ISSN 1000−7598
https: //doi.org/10.26599/RSM.2024.94300589 journal homepage: rocksoilmech.whrsm.ac.cn

Model test of deformation and failure mechanism of gravel soil bank slope under rainfall and reservoir water level

DING Jun-ling[1], JI Feng[1], WEI Song[1], ZHANG Bo[2], ZENG Rui[1], LI Zhuo[1], LU Yu-peng[1]

1. State Key Laboratory of Geohazard Prevention and Geoenvironment Protection, Chengdu University of Technology, Chengdu, Sichuan 610059, China
2. China Railway Changjiang Transport Design Group Co., Ltd., Chongqing 401121, China

Abstract: Deformation of the deposit bank slope is intensified due to reservoir water regulation and rainfall, threatening reservoir operation. To investigate the deformation and failure mechanisms of bank slopes, as well as their infiltration characteristics, a large-scale physical model test was conducted to simulate rainfall and its interactions with water level fluctuations at the Sanbanxi Reservoir in Guizhou Province. The parameters such as pore water pressure in slope and the whole process of slope deformation evolution are obtained. The results show that: (1) The final shape of the modeled wetting front is determined by the slope shape, and the different infiltration effects are mainly manifested in the change of migration depth, and the seepage field characteristics and slope gradient have a greater influence on the migration rate. (2) The soil pressure curve changes gently under both conditions, the pore water pressure changes with a lag, and the soil pressure and pore water pressure in the deeper layers of the slope body fluctuate more than those in the shallower layers in the saturated state. (3) Slope deformation during rainfall is dominated by erosion pits and localized slides, while erosion gullies dominate during coupling, and the scale of slope erosion during coupling is about twice as large as that during rainfall, but multi-stage slip traction damage occurs at the foot of the slopes in both conditions. (4) Based on the experimental results, the deformation and damage mechanism of the modeled bank slope under the coupled rainfall and water level is summarized into five stages: softening and settling of the slope surface, development and expansion of erosion rills, and development of erosion gullies and collapse at the foot of the slope. The results of this study fill the gap in the study of bank slope stability under the above conditions in Sanbanxi Reservoir area, and it is useful for the study of similar deformation damage of gravel soil bank slopes and their prevention and control.

Keywords: rainfall and reservoir water level; gravel soil bank slope; model test; deformation and failure mechanism; infiltration features

1 Introduction

In recent years, the advancement of hydropower project construction in China has drawn significant attention to bank slope instability and its associated engineering impacts[1−2]. The reservoir areas are mostly located in the alpine canyon area, where the geological settings are complex, and the unstable slopes are highly developed on both banks[3]. Compared to mountain slopes, bank slopes are influenced not only by fundamental sliding factors but also by various boundary conditions, such as reservoir water infiltration and wave effects[4]. The fluctuations resulting from the scheduling of reservoir water can easily lead to deformation and failure of the bank slope. This risk is exacerbated under external influences, such as occasional rainstorms, which significantly increase the likelihood of destabilization. In this context, it is essential to investigate the deformation and failure mechanisms, as well as the evolution processes of deformation, and the seepage characteristics of bank slopes influenced by reservoir water regulation and rainfall will be crucial for the prevention and control of geological disasters in the reservoir area[5−6].

Since 1987, Gatto and Doe[7] have proposed that the bank slope collapse should be treated as a specific location problem, numerous studies have been conducted on bank slopes in this regard. Studies have shown that the mechanism of water action on slopes is mainly manifested in weakening the shear strength of the slope material[8] which is manifested in putting the slope in a state of high water saturation, changing the stress distribution, decreasing the effective stresses, fragmenting the soil particles and causing the slope to settle[9−11]. In addition to the above mechanisms, reservoir impoundment also leads to the deterioration of the slip zone strength and significantly reduces the stability of bank slopes[12−14].

In light of the cases involving the deformation and failure of bank slopes under the combined effects of rainfall and water level fluctuations, research is typically conducted through field monitoring, numerical simulations, and physical modeling tests[15−17]. Field monitoring, based on the changes in slope displacement, can be utilized to analyze the deformation characteristics and development trends of slopes. The results obtained from such monitoring can serve as a reference for similar studies[18]. Summarizing the results of numerous field monitoring studies on slopes,

Received: 17 December 2024 Accepted: 14 April 2025
This work was supported by the National Natural Science Foundation of China (41977273).
First author: Ding Junling, male, born in 1999, doctoral student, mainly engaged in the study of geological disaster stability prediction and evaluation. E-mail: dingjunling@stu.cdut.edu.cn
Corresponding author: Ji Feng, male, born in 1980, PhD., Professor, doctoral Supervisor, mainly engaged in the research on the prediction and evaluation of the stability of major geological disasters. E-mail: jeifens@163.com

it is evident that the deformation of the shallow slope body is primarily controlled by rainfall, with the deformation rate being directly proportional to the intensity of rainfall. In contrast, the deep slope body is significantly influenced by water level fluctuations, with its deformation rate being directly proportional to both the amplitude and rate of water level changes[19]. In addition, only from the perspective of water level fluctuation, it can be seen that the stability of bank slope decreases first and then increases when the water level decreases, and shows a three-stage evolution law of increase-decrease-increase when the water level rises[20−21].

The numerical simulation method can effectively analyze slope deformation evolution and stress field distribution characteristics, so it is applied in many engineering cases[22]. Based on the finite difference and fluid-solid coupling effect, the influencing factors of bank slope stability such as rainfall mode and slope permeability can be obtained, and the variation characteristics of relevant parameters in the evolution of bank slope deformation can also be obtained[23−25]. With the help of relevant simulation software, we can analyze the mechanism of rainfall and water level fluctuation on the deformation and damage of bank slopes, and we can also know the prediction and calculation methods of bank slope instability, such as calculating the safety factor and locating the most dangerous slip surface[26−27].

Physical model testing can effectively replicate the entire process of slope instability while simultaneously monitoring and recording the evolving characteristics of multi-field information throughout this process. Currently, it has emerged as a crucial method for investigating the deformation and failure mechanisms of bank slopes[28−29]. The model test of bank slope under the coupling of rainfall and water level fluctuation can reveal the deformation and failure mechanism of bank slope and the evolution law of mechanical parameters[30−33]. The results of many model tests show that under the combined action of reservoir water level fluctuation and rainfall, the overall effective stress of the bank slope decreases, the shear strength of the infiltrated soil decreases, the seepage pressure increases, and the deformation of the bank slope concentrates on the leading edge of the slope and shows the characteristics of traction failure[21, 34−35].

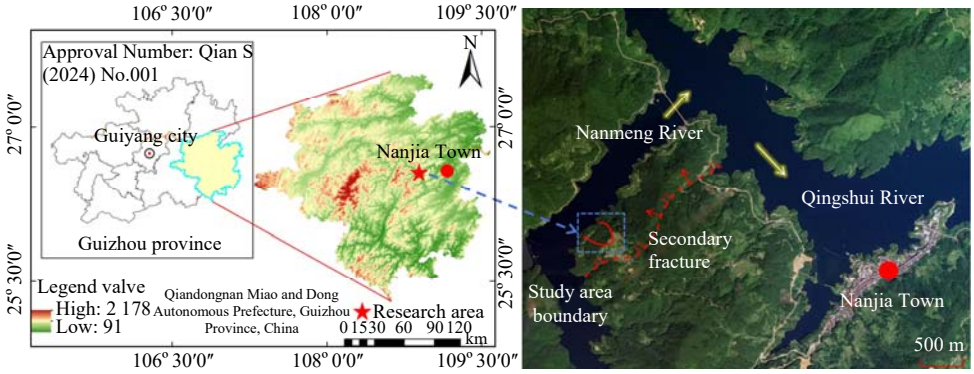
In summary, current research on bank slope model testing mainly uses rock or homogeneous materials for slope model tests, fewer studies have been conducted on predominantly in-situ soil-rock mixes. In addition, most of the studies are based on landslides or large-scale deformation of bank slopes, while ignoring the localized collapse at the foot of slopes that develops in a gradual traction manner, resulting in the possibility of overall destabilization of the bank slopes. In light of this gap, this study adopts the in-situ gravel soil from the deposit bank slope in the Sanbanxi Reservoir area as its material. Taking into account extreme working conditions, an indoor model test was designed to investigate both the deformation and failure mechanisms as well as the infiltration characteristics of the bank slope under uniform intensity rainfall and its interactions with water level fluctuations. This study provides valuable insights into the instability characteristics of the bank slope along the Qingshui River, which is of some reference significance for the research related to the bank slope of the accumulation body with steep slope and thick cover layer, but there is still the possibility of destabilization, and it is also important for elucidating the evolution of deformation processes and understanding the disaster mechanisms associated with gravelly soil bank slopes.

2 Geological survey and model generalization

The bank slope of the accumulation body is located in Qiandongnan Prefecture, Guizhou Province (Fig. 1). This region has a humid subtropical monsoon climate, with an average annual temperature of 16.7 ℃. Rainfall averages 1 226.4 mm annually, with a maximum of 73.44 mm in one day. Precipitation mainly happens in early summer and varies greatly across the region. The elevation of the leading edge of the bank slope is 431.5 m, and has a certain slope change. The elevation of the trailing edge is 606 m, and the terrain is gentle. The left side is bounded by a gully, with gray tuffaceous slate exposed and joints and fissures outside the gentle slope developed. The right side is a gully without bedrock exposed.

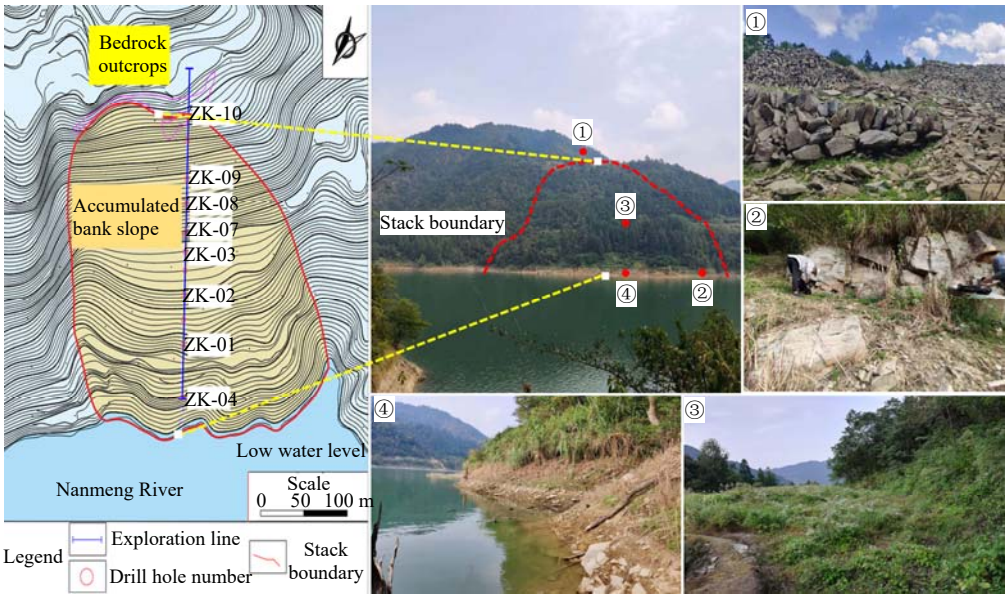
According to the exploration line drilling, the maximum depth of the bank slope's leading edge is measured at 27.7 m, while the maximum depth of the middle platform is approximately 30.8 m, and that of the trailing edge reaches up to 33 m. The area encompasses an estimated 6.88×10^4 m^2, with a corresponding volume of about 1.307×10^6 m^3. The plane shape extends fan-like towards the northwest, characterized by a profile reminiscent of a ladder. The slope consists of forested areas and abandoned agricultural land (Fig. 2). The segment extending from the front edge of the bank slope to the central platform is primarily composed of gravel soil, interspersed with layers of silty clay and lenses of block stone soil. The surface layer at the trailing edge consists of silty clay, while deeper strata are predominantly characterized by block stone soil, accompanied by occasional lenses of gravel and silty clay.

According to the characteristics of the bank slope's wading area and on-site observations, vegetation density is low in both the middle and lower sections. The surface gravel is notably fragmented and accumulates extensively, while erosion gullies and collapses along the bank slope are particularly prevalent. This suggests that this section



(a) Terrain (b) Satellite image

Fig. 1 The geographical location of Nanmeng River accumulation body



Note: ① Slope trailing edge artificial masonry; ② Bedrock outcrops at the front edge of the slope; ③ Gentle platform in the middle of the slope; ④ Local collapse of slope toe.

Fig. 2 Plane illustration of Nanmeng River accumulation body

is significantly influenced by rainfall and reservoir water levels. Consequently, selecting it as a model object minimizes the effects of vegetation and other variables, thereby enhancing the reliability of the model test outcomes.

In this context, the elevation of the exploration line 2-2 section below 540 m (Fig. 3) is selected as the subject for constructing a bank slope model grounded in similarity theory. Utilizing gravel soil as the modeling material and considering the testing conditions, a similarity ratio of 1∶200 has been established for the model. The designed bank slope possesses a height of 0.45 m and a length of 1.20 m, with inclination angles at the front and rear measuring 30° and 33°, respectively.

3 Materials and methods

3.1 Similarity conditions and model materials

The model is constructed by following five similarity conditions, i.e., geometry, material, hydrodynamic characteristics, boundary conditions and similarity of motion[36], while local geometric similarity and environmental factors are secondary factors. In light of the effects of testing conditions and size variations, this experiment employs an incomplete similarity simulation methodology, that is, considering the main factors while ignoring the secondary factors. The relationships of similarity between the prototype and the model physical quantities pertaining to bank slope are delineated in the following formula and Table 1.

$$C_\gamma = C_v = C_\mu = C_\theta = C_k = 1 \tag{1}$$

$$C_q = \sqrt{n} = 10\sqrt{2} \tag{2}$$

$$C_h = C_l = C_t = n = 200 \tag{3}$$

where C is similarity ratio, γ is unit weight, v is velocity,

μ is the Poisson's ratio, θ is volumetric water content, q is rainfall intensity, k is permeability coefficient, n is the geometric similarity ratio, h is height, l is length, and t is time.

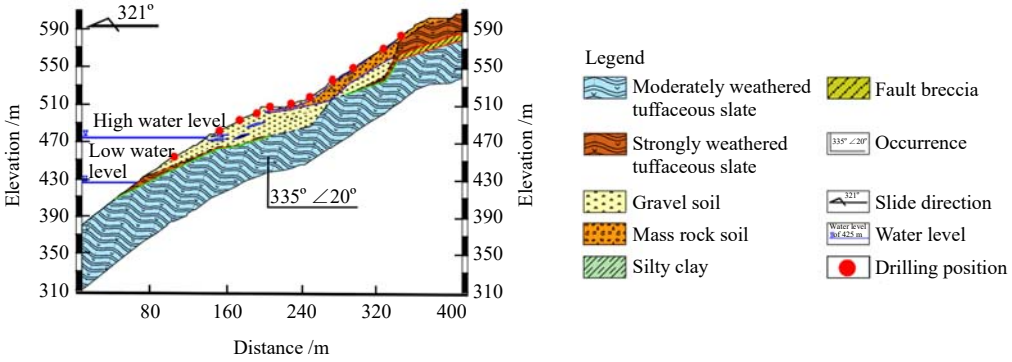


Fig. 3 Engineering geological profile of accumulation

Table 1 The similarity relationship between the model and the prototype physical quantity

Stress(σ)	Velocity(v)	Lateral pressure(p)	Internal friction angle(φ)	Cohesion(c)	Time(t)	Height(h)	Length(l)	Density(ρ)	Gravity(g)	Deformation(ε)	Volumetric water content(θ)
1	1	1	1	1	200	200	200	1	1	1	1

The soil utilized in this study primarily comprises gravelly mixed soil, sourced from the bank slope of the Nanmeng River. Some physico-mechanical parameters of the prototype and model are presented in the following Table 2. According to the relevant standards outlined in Standard for geotechnical testing method (GB/T 50123—2019)[37], the model width b and particle size d_m should meet $25<b/d_m<40$. In order to ensure the uniformity of the model and eliminate the particle size effect, the particle size of the model soil is required to be less than 20 mm according to the standard. Therefore, it is necessary to use the equivalent substitution method to replace the super-sized particles with small-sized particles. The specific principle can be seen form formula (4).

$$P_i = \frac{P_{oi}P_5}{P_5 - P_{d\max}} \tag{4}$$

where P_i is the content of a particle size group in the soil after replacement, P_5 is the content of soil particles larger than 5 mm, $P_{d\max}$ is the content of particles in the super particle size group, and P_{oi} is the content of a particle size group in the original soil.

After the transformation of formula[4], the resulting gradation of the final model material particles is presented in Table 3.

Table 2 Parameter values of basic physical and mechanical properties of prototype and model

Name	Unit weight /(kN·m^{-3})	Moisture content/%	Permeability coefficient /(cm·s^{-1})	Cohesion /kPa	Internal friction angle /(°)
Prototype slope	19.465	28.3	3.01×10^{-3}	24.0	30.0
Model slope	19.701	28.7	3.23×10^{-3}	22.1	29.2

3.2 Test systems and modeling

The main device features a custom glass sink measuring 150 cm×40 cm×50 cm (Fig. 4). The testing system consists of three components: rainfall, water level fluctuations, and model monitoring. The rainfall system is positioned on the steel frame above the model box, whereas the water level lifting system is situated at the front bottom of the box. Both rainfall intensity and water elevation rate are regulated by a combination of a pump and a flowmeter. The model monitoring system comprises sensors that measure water content, matric suction, soil pressure, and pore water pressure within the slope. Additionally, it includes external laser displacement sensors, cameras, and a Pentax 3D laser scanner. The parameters of each monitoring instrument are shown in Table 4.

Table 3 Substitution table of particle size distribution

Particle size/mm	Percentage contents/%	
	Original sample	Treated sample
20−10	10.11	13.35
10−5	9.95	13.14
5−2	28.64	37.82
2−1	14.16	18.70
1−0.5	2.27	3.00
0.5−0.25	4.05	5.35
0.25−0.075	3.07	4.05
<0.075	3.48	4.60

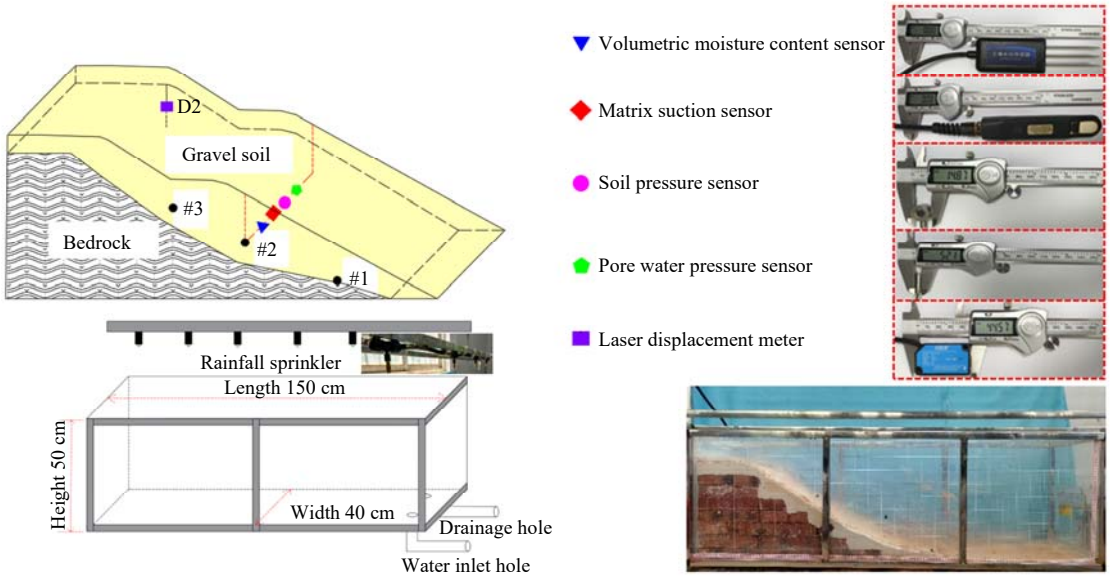


Fig. 4 Model box, schematic diagram of the model, and related monitoring instruments

Table 4 Specifications and related parameters of monitoring devices

Monitoring device	Model	Number	Precisions	Measurement range
Pore water pressure	HC-25	3	0.2% F.S	−10−15 kPa
Soil pressure	HC-16	3	0.2% F.S	0−75 kPa
Moisture content	C-5	3	±3%	0%−100%
Matrix suction	TENSIOMARK	3	±0.35 pF	7−0 pF
Laser displacement meter	HC-XX	2	70 mm	0−35 mm
3D laser scanner	PENTAX ｜ S-3180	1	0.007°(RMS)	0.3−206 m

Note: RMS stands for root mean square, used to represent the effective value or standard deviation of data.

A total of three monitoring points are established in the model to acquire real-time mechanical parameters, including slope surface displacement and pore water pressure. Two slope surface displacement sensors, denoted as DX, are installed on the outer slope. Four types of sensors are deployed on the inner slope, designated as PX, SX, MX, and WX to represent pore water pressure, earth pressure, matrix suction, and moisture content, respectively, where X denotes the serial number of each monitoring point, where matrix suction is employed to validate the accuracy of pore water pressure data collected. The location of each monitoring point and sensor is shown in Fig. 5.

Based on the design and dimensional requirements of the bank slope in Fig. 5, the physical model was selected to be constructed directly in the model box. The model should be calibrated and the sealing of the model box should be tested before the model is made, and it can be stacked only after the test is qualified. The test site is a laboratory, and the test conditions are based on the natural environmental parameters of the study area during the rainy season, and the test temperature is finally determined to be 22−28 °C, and the humidity is maintained at 75%−85%.

Bedrock modeling: First, the contours of each section were drawn on the outside of the model box and the locations of the monitoring points were marked. The main part of the bedrock model is constructed with bricks, in which the interface of the bedrock model needs to be covered with gypsum mortar and browned. After the gypsum mortar is solidified, the inner wall of the glass box and the bedrock model should be coated with glass glue to achieve the effect of water insulation.

Slope modeling: Firstly, the mass of gravel soil required for the model slope should be calculated according to the contour of the gravel soil bank slope and its weight capacity, and the corresponding mass should be weighed and dried, then crushed and sieved, and then the gravel soil mixture should be calculated and proportioned according to the above requirements on the particle size, and then the moisture content of the mass should be adjusted to 28.3%. Afterwards, in order to minimize the friction between the slope and the inner wall of the glass box during the test, petroleum jelly was applied to the contact area between the inner wall of the glass box and the modeled slope. The soil was compacted in layers of 4 cm thickness, and the mass and volume of the compacted soil were calculated for each layer to ensure that the density of each layer was 1.95 g/cm^3. In this process, the in-slope sensors were buried at the monitoring markers on the outside of the model box. After the model stacking is completed, the surface of the slope model needs to be

smoothed and sloped to ensure that the uniformity of the slope surface is equal, and then sprayed with a small amount of rain spray and left to stand for more than 12 h. Finally, the off-slope monitoring system is installed in accordance with the designated monitoring points. Finally, the off-slope monitoring system was set up according to the specified location, and the test system was set up as shown in Fig. 6.

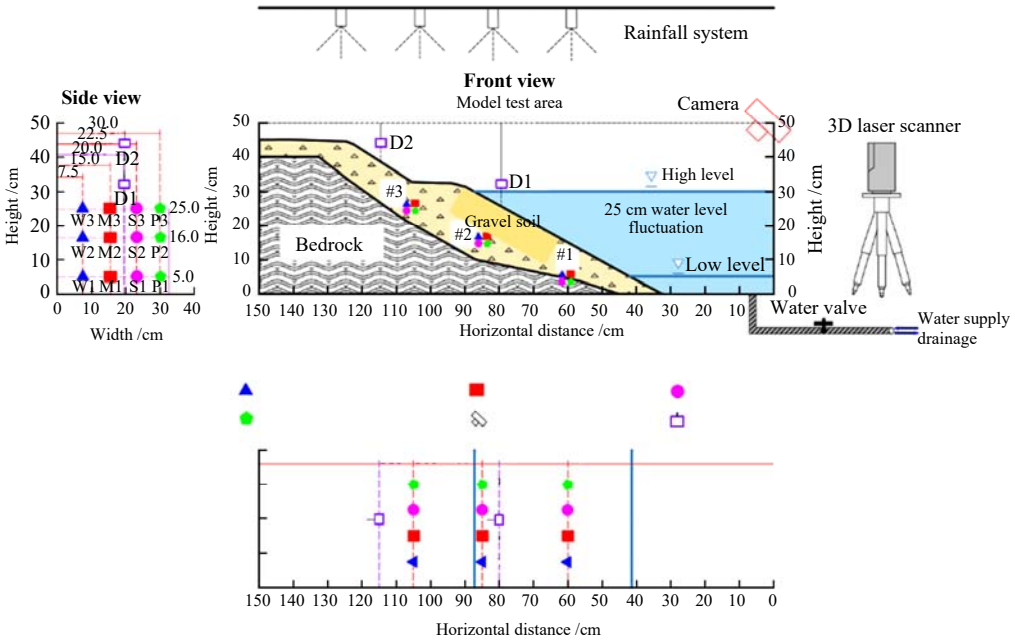


Fig. 5 Monitoring layout of physical test model

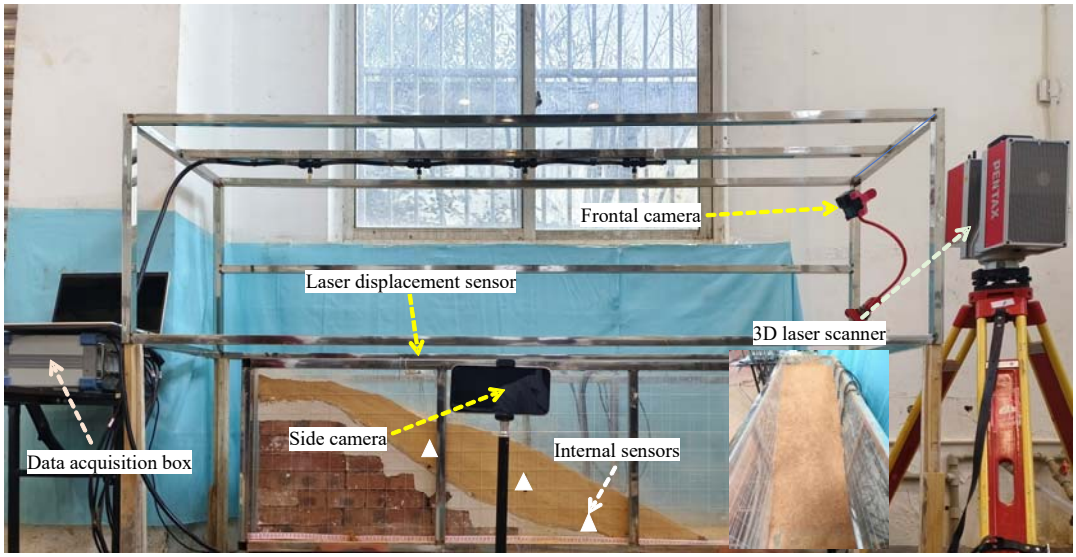


Fig. 6 Deployment of monitoring devices for physical test models

3.3 Test scheme

According to local meteorological and hydrological data, extreme conditions under two scenarios were selected based on the operational parameters of the reservoir area. The rainfall intensity of the rainfall is determined by the maximum daily rainfall recorded since the reservoir became operational, while the duration of rainfall is established using calculation results related to both precipitation and model water capacity. The rate of water level rise and fall in the model is designed according to the minimum dispatch cycle for reservoir water levels. The test plan with prototype parameters converted by similarity relations is shown in Table 5.

4 Results

4.1 Condition 1: equal intensity rainfall

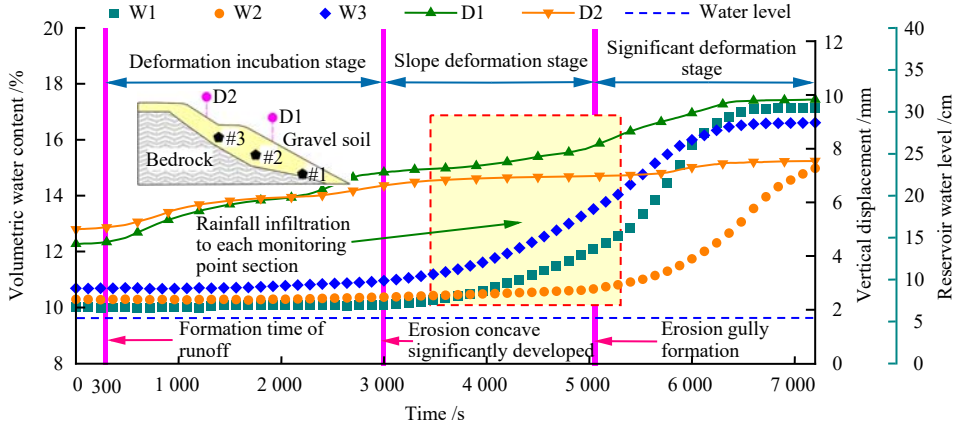
Maintaining the minimum water level of 5 cm, the rainfall intensity of 0.22 mm/h lasted for 2 h, to study the characteristics of deformation and damage of bank slopes under equal intensity rainfall, and the monitoring data are shown in Fig. 7.

Table 5 Model test condition design

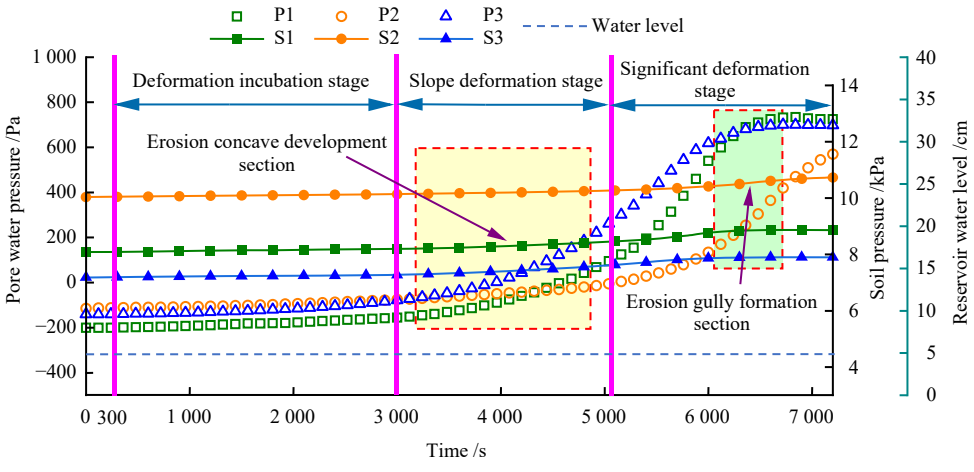
Conditions	Test condition	Prototype boundary condition combination	Model test conditions
1	Rainfall effect	425 m standing water level + full process rainfall (~3.06 mm/h)	5 cm standing water level + full process rainfall (~0.22 mm/h)
2	Coupling effect of rainfall and water level	Water level rises/falls at an average rate of 5.04 m/d, 425 m $\xrightarrow{10\ d}$ 475 m (~13 d) $\xrightarrow{10\ d}$ 425 m (~7 d) + Rainfall during water level decline (~3.06 mm/h)	Water level rises/falls at an average rate of 5.04 m/d, 5 cm $\xrightarrow{1.15\ h}$ 30 cm (~1.53 h) $\xrightarrow{1.15\ h}$ 5 cm (~0.85h) + Rainfall during water level decline (~0.22 mm/h)

Note: → indicates the duration of water level fluctuation; ~ indicates the duration of water level stability

It can be observed from the Fig. 7 that the overall trend in soil pressure and pore water pressure at each monitoring point is similar, both exhibiting a lag in response to infiltration. Moreover, there exists a strong correspondence between the characteristics of the water content curve and pore water pressure, so the reliability of monitoring data is verified. The initial soil pressure value and its response time of each monitoring point are proportional to the depth of the monitoring point, the #2 monitoring point has the longest seepage path, the wetting front arrives the latest, and due to the limitation of the rainfall duration, the nearby soil is still not saturated until the end of the test. #1, #3 pore water pressure and soil pressure change trends are similar, the value of which are in the first period of slow increase, the surge of the middle period, and the later period of smooth fluctuation, but because #1 is located at the foot of the slope, it is affected by runoff and reservoir water more, so its mechanical values change more widely. However, because #1 is located at the foot of the slope, it is affected by runoff and reservoir water, so its mechanical values have a greater variation. Eventually, the change of soil pressure of #1 is 0.91 kPa, #2 is 0.73 kPa, and #3 is 0.83 kPa, which indicates that the middle and lower part of the slope is most affected by the infiltration of rainwater, and most of the particles carried by the runoff on the slope surface are accumulated here. However, in terms of the numerical curve of earth pressure at each monitoring point, the overall trend of the curve changes gently without obvious sudden change, because the numerical value of earth pressure at the monitoring point depends on the change of the weight of the overlying soil body, so it



(a) Moisture content and slope surface displacement

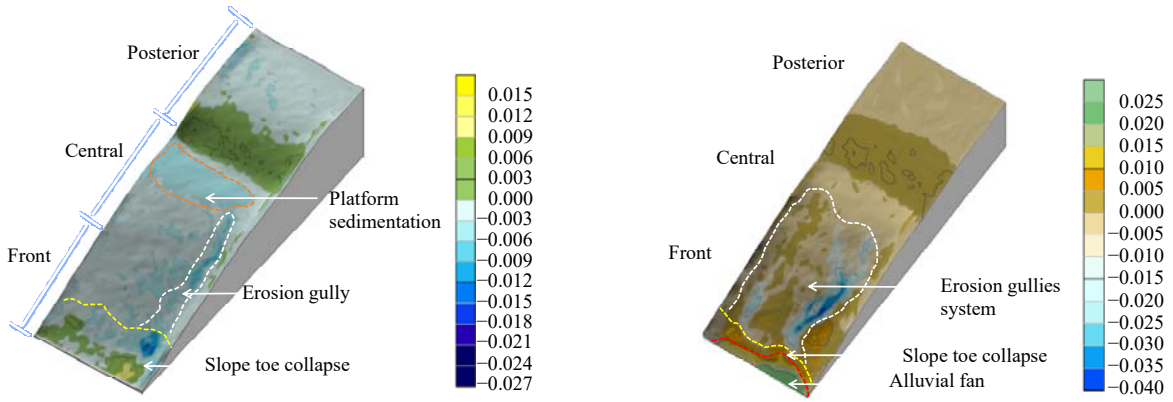


(b) Pore water pressure and earth pressure

Fig. 7 Sensor data curves of each monitoring point under condition 1

can be shown that the weight of the slope changes uniformly in this condition, i.e., the deformation of the slope surface is slow and the signs of deformation are mild, and the effect of stress redistribution is weak.

The partial displacement of the slope surface is shown in Fig. 7(a), and an increase in displacement represents the downward movement of the soil body, and vice versa. Under the effect of rainfall scouring and infiltration, the change of D1 in the middle of the slope was 5.37 mm, and the largest change was observed in the sections of 2 100−3 000 s and 5 000−6 000 s. The first section was caused by the scouring of the loose soil on the slope surface after the formation of the runoff, and the second section was caused by the increase of the erosion scale after the erosion pit was penetrated. The change of D2 in the back part of the slope is only 2.54 mm, except for the rapid increase in the early stage, and then it is a slow increase. The 3D laser scanner scanning results can be calculated and processed to produce a 3D model of the slope surface displacement change (Fig. 8), which can be analyzed in conjunction with Fig. 12 to show that there is a spatial and temporal inhomogeneity in the deformation of the slope surface under this condition. In time, the deformation evolution is concentrated in the slope surface after the formation of runoff and before the stabilization of the erosion gully (300−6 300 s), while in space, it is concentrated in the middle and front part of the slope, with the displacement of the collapse of the foot of the slope in the front part of the slope being about 6−15 mm, and that of the erosion gully in the middle part of the slope being about 6−12 mm. In order to make it easier for the comparison and analysis of the results of calculations for the condition 2, the present study focuses on the scale of the erosion of the segment of the slope body belowthe vertical height of 30 cm in the model. After calculation, the erosion area in this case accounts for about 39.3% of the total area of this section, and the erosion volume is about 885 cm^3, which accounts for 10.5% of the total volume of this section of the slope. About 45% of this eroded volume was located on the left side of the slope in this section and spread around the erosion gully, and about 50% was located at the foot of the slope and concentrated at the gully entrance of the erosion gully. In addition, the foot of the slope had an accumulation of about 502 cm^3, of which 62% was also located near the gully entrance. It can be seen that the formation of the erosion gully has a great influence on the amount of erosion on the slope surface and the accumulation at the foot of the slope, and at the same time, its location determines the distribution of the erosion concentration



(a) Condition 1 (b) Condition 2

Fig. 8 Three-dimensional laser scanning results of surface displacement on model slope (unit: m)

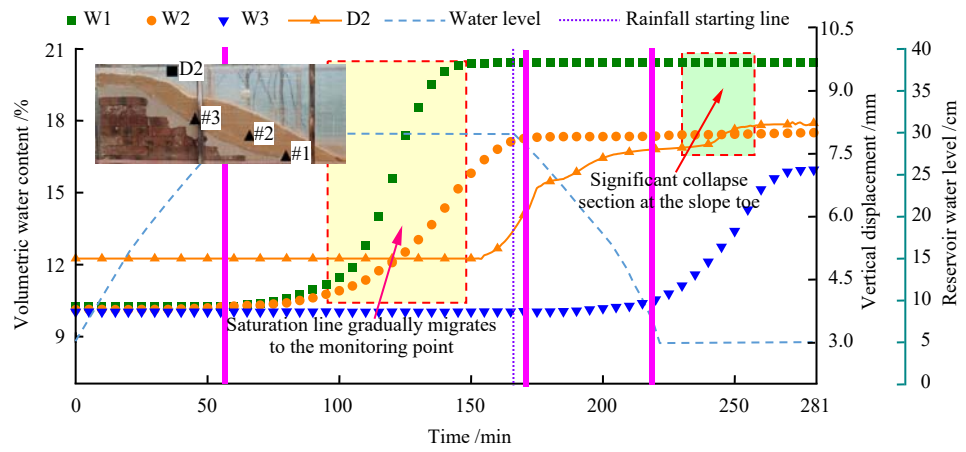
area on the slope surface.

4.2 Condition 2: coupled hydro-mechanical effect

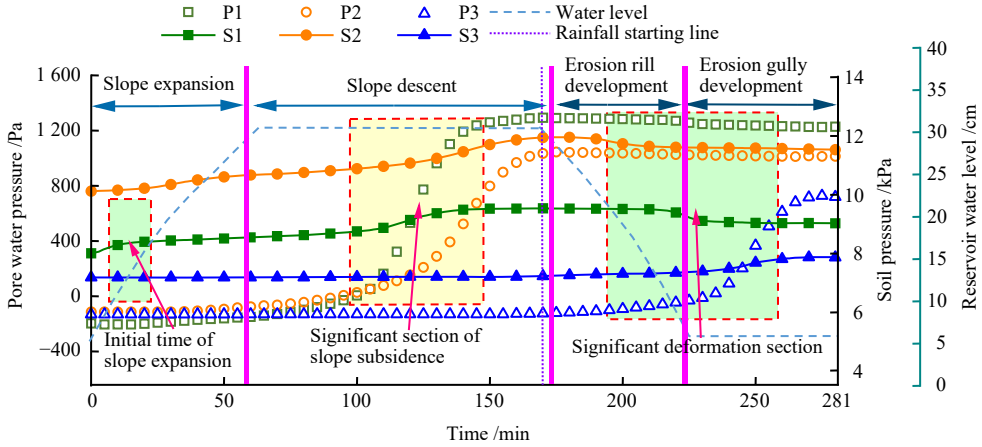
This study investigates slope deformation characteristics and mechanisms under rainfall and varying water levels, as per design requirements for condition 2. Monitoring data are shown in Fig. 9.

Figure 9(a) shows during the stage of water level rise and highest water level stabilization, the water content of the reservoir flooded zone shows the trend of slow increase-surge-stabilization due to the infiltration of the reservoir water, with the peak values of W1 is 20.43% (3.33% higher than condition 1) and that of W2 is 17.51% (2.53% higher than condition 1). Thus, it can be seen that the amount of infiltration of condition 2 is larger than that of condition 1, which is mainly caused by the fact that reservoir water is more than the rainwater by gravity. When the water level decreases and stabilizes at a low level, W1 fluctuates steadily due to soil saturation, W2 increases slowly due to the continuous rainfall infiltration, and W3 is similar to condition 1 but with a final increase of about 0.3%.

It can be seen from Fig. 9(b) that compared with P1, P2 has a longer seepage path, the change amplitude is only 80% of that of P1, which has a long seepage path



(a) Moisture content and slope surface displacement



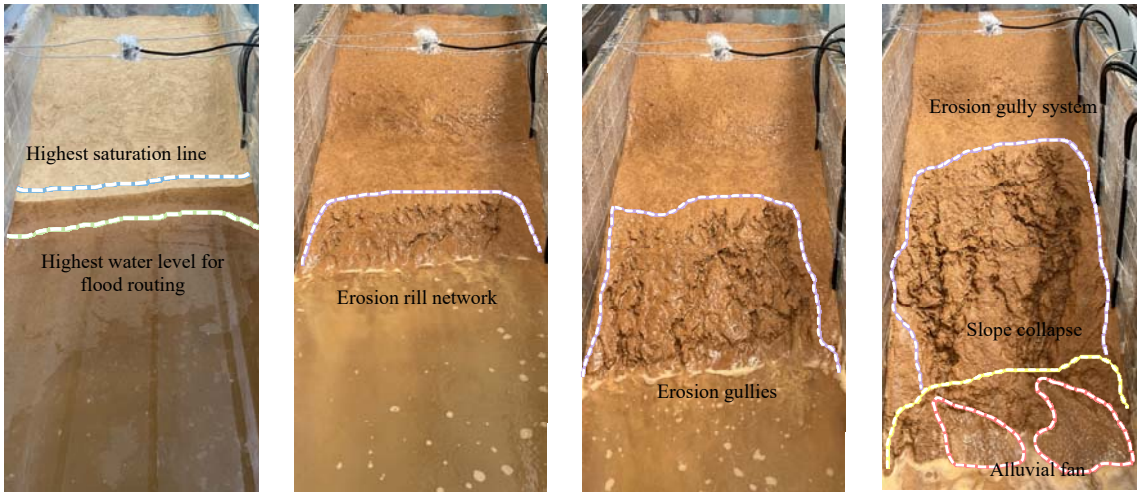
(b) Pore water pressure and earth pressure

Fig. 9 Sensor data curves of each monitoring point under condition 2

and a long response time to reservoir water fluctuations, with a slightly lower change amplitude, and is less affected by water level fluctuations and rainfall. Because P1 is located at the base-cover interface and the buried depth is shallow, it has a rapid response to the infiltration of the reservoir water, and the change range is the largest, which is significantly affected by the water level. The change processes of P1 and P2 with water level fluctuations are similar. Both increase slowly as the water level rises and sharply when reservoir water infiltrates the monitoring point. The water level decreases and increases first and then decreases with rainfall, and the lowest water level is stable. Due to the fact that P3 remains unaffected by fluctuations in water levels, its trend of change closely mirrors that of the condition 1.

According to the analysis of the soil pressure curve, the soil pressure at monitoring point #1 changes first and reaches its peak because it is the first to bear the gravity and infiltration of the reservoir water. #2 is located in the middle of the slope, the soil pressure rise is the largest, but the overall rate of change is small, its curve changes gently. The final change of S1 is 1.1 kPa, with an increment of 0.3 kPa compared with condition 1, and S2 is 1.4 kPa, with an increment of 0.7 kPa, which indicates that the change of slope weight in condition 2 is larger than that of condition 1, and this reflects its greater influence on slope stability. The soil pressure trend at #3 is similar to condition 1, but S3 responds earlier due to reservoir capillary force. The rainfall infiltration delay is slightly reduced, and the final peak value is 0.24 kPa higher than in condition 1.

The change of D2 displacement is basically the same as that of condition 1, but the capillary effect of reservoir water causes its value to change in 7 min before the rainfall, and the maximum displacement increases by about 0.4 mm. From Figs. 8(b) and 10, it can be seen that the deformation of the reservoir flooded zone under this case is intense. When the water level rises and the high water level stabilizes, there is no obvious sign of deformation on the slope except for a slight expansion and settlement. However, when the water level drops, the deformation of the submerged zone is especially significant. At the early stage of water level decline, the erosion of the rills are very developed, and due to runoff erosion and gradually



(a) Peak water level (b) Mid-stage of water level decline (c) Late stage of water level decline (d) End of experiment



(e) On-site erosion gully (f) On-site slope toe deposition (g) On-site reservoir bank collapse

Fig. 10 Evolution process of model slope surface deformation under condition 2

evolved into erosion gully, at this time, the dry and wet interface at the cracks are also due to rainfall erosion and gradually deepen. During this process, the descending drag of the reservoir water and rainfall scouring lead to the soil on the slope being transported to the reservoir water, resulting in the collapse of the slope and turbidity of the reservoir water. At the same time, the infiltration pressure also pushes out the air-water film from the slope surface, resulting in foaming on the reservoir surface. When the minimum water level is stabilized, the foot of the slope is subject to retroactive erosion and discontinuous cracks are generated, which are gradually penetrated under continuous rainfall, and ultimately lead to small-scale pile-ups at the foot of the slope and multi-stage sliding surface sliding phenomenon. After calculation and analysis, it can be seen that the deformation of the slope under this condition is concentrated in the reservoir flooded section, in which the maximum displacement of the erosion gully reaches 40 mm, and the displacement of the foot of the slope partially collapsed is about 5−15 mm, and the erosion area accounts for 78.6% of the total area of the section, and the erosion volume accounts for about 1 920 cm^3, which accounts for 22.9% of the total volume of the slope body, and the accumulation of the foot of the slope is about 805 cm^3. The distribution and scale of erosion and accumulation areas in both conditions are compared and found to be the same as that of the slope. After comparing the distribution of erosion and accumulation areas and their sizes under the two conditions, it is found that the distribution of erosion and accumulation areas in both conditions is located near the erosion gully, but there are differences in the location and development pattern of the erosion gully. Meanwhile, the scales of the erosion gully and the foot of the slope collapse and its accumulation at the mouth of the gully in condition 2 are obviously larger, but the ratio of the amount of the collapse volume to the accumulation volume is smaller than that of the condition 1, which is mainly due to the fact that most of the erosion material is carried away by the trailing of the falling water from the reservoir.

4.3 Mann-Whitney U analysis of pore water pressure and soil pressure data

To make the comparative more analysis intuitive, the statistical results of soil pressure and pore water pressure changes at monitoring points are shown in Fig. 11, from the figure can be seen, the monitoring points of soil pressure change amount is slightly larger than the pore water pressure, and for condition 2 this trend is smaller than the condition 1. According to the principle of Terzaghi effective stress, the difference between the soil pressure and the pore water pressure that is, the effective stress, which is known that the condition 2 under the action of the slope body. It can be seen that the effective stress

decreases at each location under condition 2, which proves that the coupling of rainfall and water level has a greater impact on slope stability than single rainfall.

In addition, taking the rainfall condition as the control group and the water level fluctuation and rainfall coupling as the experimental group, the Mann-Whitney U test was conducted to analyze the soil pressure and pore water pressure data of each monitoring point to increase the persuasive power of the relevant conclusions. The #3 monitoring point is not affected by the water level fluctuation, in order to ensure the reasonableness of data analysis, so only selected its condition 2 rainfall section of the data to analyze, the results of the calculations are shown in Table 6. It can be seen from the figure, the coupling of water level fluctuation with rainfall, the *p*-value of the P1, P2, S1 and S2 are all less than 0.05, thus indicating that the coupling of water level fluctuation with rainfall is a very important factor in the development of the water table. This shows that the coupling of rainfall and water level has a significant effect on the pore water pressure and soil pressure change characteristics of the modeled slopes compared to the rainfall only. The *p*-value of pore water pressure and soil pressure at monitoring point #2 is smaller than that of #1, and the change amplitude of the two values is also larger, which proves that the relevant parameters in the deeper part of the slope body are affected by the fluctuation of the water level more. The *p*-value of P3 and S3 is greater than 0.05, because they are not affected by the fluctuation of water level, so it is verified that the consistency between the model of condition 1 and 2 is higher, the interference of other irrelevant variables is smaller, and the credibility of the experimental data and its related conclusions is larger.

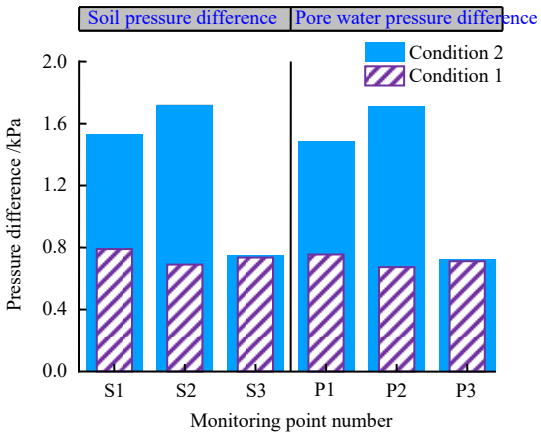


Fig. 11 Variations in pore water pressure and soil pressure at each monitoring point

Table 6 Results of Mann-Whitney U-test for pore water pressure and soil pressure

Condition	Monitoring points	Upper quartile	Mann-Whitney U-value	*Z*-valve	*p*-valve
Water level fluctuations + rainfall	P1	1.192	8 775	−7.641	2.16×10^{-14}
	P2	0.523	9 237	−7.207	5.7×10^{-13}
	P3	−0.131	7 138	−0.960	0.337
	S1	9.035	3 900	−12.213	2.65×10^{-34}
	S2	11.555	2 098	−13.904	5.977×10^{-44}
	S3	7.864	7 293	−0.685	0.493

5 Discussion

5.1 Infiltration properties and deformation characteristics under equal intensity rainfall

Figure 12 shows the morphology of the modeled lateral wetting front at different moments of condition 1, where T_1, T_2, T_3 denote the elapsed time of the experiment. The results show that with the increase of rainfall duration, the wetting front gradually migrates downward along the slope contour, and the rate gradually decreases, and the migration rate in front of the slope is larger than that in the back of the slope. This is mainly due to the smoothness of the slope surface and the uniformity of rainfall, resulting in the synchronized downward migration of the wetting peaks at all places of the slope. However, the deeper the depth of the soil body, the greater the influence of the overlying soil weight, the higher the degree of compaction, the smaller the permeability coefficient, the slower the rate of infiltration. At the same time, gravity causes the runoff on the slope surface to concentrate on the front edge of the slope, and the hydraulic gradient causes the infiltration in the middle of the slope to be directed to the front of the slope, so it accelerates the infiltration rate of the front edge. Because of the characteristics of the slope shape and rainfall duration, the final shape of the wetting front is “hump type”, i.e., shallow infiltration in the middle and deep infiltration on the side, which has obvious correspondence with the pore water pressure value changes at each monitoring point.

Figure 7(b) shows that the value of P1 decreases rapidly after a sudden rise, which is different from the change characteristics that the pore water pressure of homogeneous silty clay will continue to increase under rainfall[38]. The reason is that the rainfall infiltration is blocked by underlying bedrock, causing transient groundwater accumulation that rapidly saturates the soil near #1, leading to a sharp increase in the P1 value. Subsequently, when this point connects with groundwater at the slope’s foot, buoyancy briefly decreases the P1 value. Finally, after stabilization of the seepage field, numerical stability fluctuates. The pore water pressure at the leading edge of the slope under the action of rainfall from a slow increase

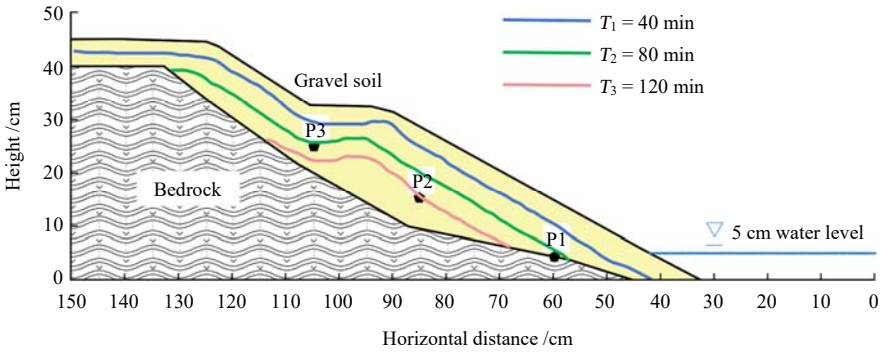


Fig. 12 Migration and evolution process of wetting front under condition 1

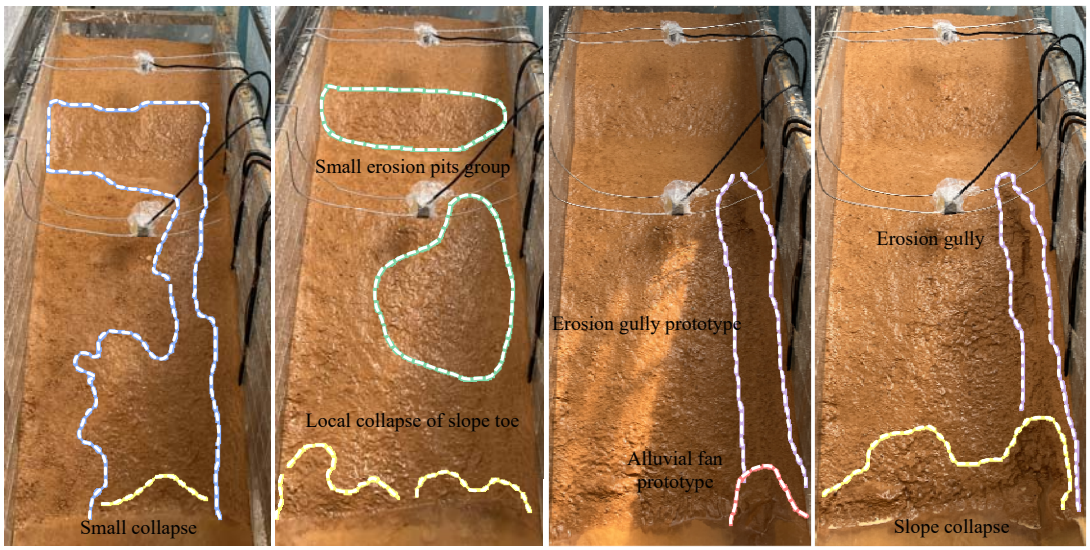
to surge, and then to a stable fluctuation stage and many slope model test results are basically consistent, thus proving that most of the slopes under the action of rainfall infiltration characteristics of similarity, that is, the pore water pressure within the slope in the early stage of rainfall basically unchanged, mainly due to the rainfall infiltration at this time the range of small, the slope of the soil body in many places are still not subjected to the infiltration of the cause. When the rainwater infiltration to the slope, most of the soil within the slope is still not saturated, in the follow-up rainwater further infiltration, the pore water pressure will be a slow increase in the trend. When the soil within the slope by rainwater infiltration for a long time after immersion will be partially saturated, then the pore water pressure of the soil within the slope in the rainwater infiltration and local deformation of the slope surface will be a stable fluctuation of the trend[39−40].

Soil pressure changes are closely linked to rainfall infiltration and slope deformation. In the early stage of rainfall, rainwater infiltrates along the void gullies in the slope, the soil body increases in weight, and the soil pressure increases slowly. When the rain water infiltrates into the place where the sensor is buried in the middle and late stages of rainfall, the soil pressure is increased due to the tight arrangement of the soil, and the stress redistribution is caused by the deformation of the slope, resulting in a sharp increase in soil pressure. Subsequently, when the soil around the monitoring point reaches partial saturation and slope deformation stabilizes, soil pressure fluctuations become mild. However, if the slope undergoes large-scale deformation or a shift, there will be a notable decrease in soil pressure. In this regard, the idea of exploring the water seepage characteristics in the slope and the deformation and failure of the slope surface based on the variation characteristics of soil pressure can provide a basis for the early warning of bank slope instability[3].

As can be seen from Fig. 13, at the beginning of the rainfall period, runoff from the slope surface was formed, and fine-grained materials were transported and accumulated in localized areas at the foot of the slope, resulting in an increase in weight and water content, a decrease in shear strength, and the occurrence of small-scale landslides under the action of subsequent runoff. In the middle and late stages of rainfall, localized landslides and erosion pits were prominent, and continuous rainfall erosion led to the passage of erosion pits with obvious gully characteristics, and the scale of the foot of the slope collapse increased and developed retrospectively. Finally, the erosion gully passes through, and obvious collapse can be seen at the gully mouth, which is mainly due to the fact that after the erosion gully passes through, the runoff will be converged in the gully, resulting in increased erosion at the mouth of the gully, coupled with the foot of the slope shear strength due to the long-term rainfall scouring and reduced, so there is obvious collapse phenomenon at the mouth of the gully. At the same time, the right side of the foot of the slope has a localized bulge, which is mainly due to the existence of a dominant seepage gully here, and the significant performance of pipe surge-type submerged erosion, leading to the accumulation of fine-grained materials here and bulge, and subsequent rainfall will occur under the action of the landslide. However, for the slope as a whole, because the design of this condition is of equal strength and continuous rainfall, coupled with the fact that there are no original cracks and other infiltration recharge gullies at the back edge of the slope, and the overall slope gradient is slower, the slope is thicker, and the slope has a larger value of c and φ. Therefore, the modeled slope has not slid as a whole under rainfall, and there is no large-scale landslide phenomenon, which is more in line with the actual situation of most of the bank slopes of accretionary bodies[29, 41].

5.2 Seepage characteristics and deformation failure mechanism under the coupling of rainfall and water level

As can be seen from Fig. 14, when the water level rises and the highest water level stabilizes, the modeled wetting front migrates synchronously in multiple directions under the influence of hydraulic gradient and gravity, and the trend of longitudinal migration is the strongest. When the water level decreases and the lowest water level stabilizes, the migration scale of the wetting front in the slope of the reservoir submerged section increases only slightly, while the change characteristics of the



(a) Initial rainfall (b) Mid-rainfall (c) Late rainfall (d) End of rainfall

Fig. 13 Evolution process of model slope surface deformation under condition 1

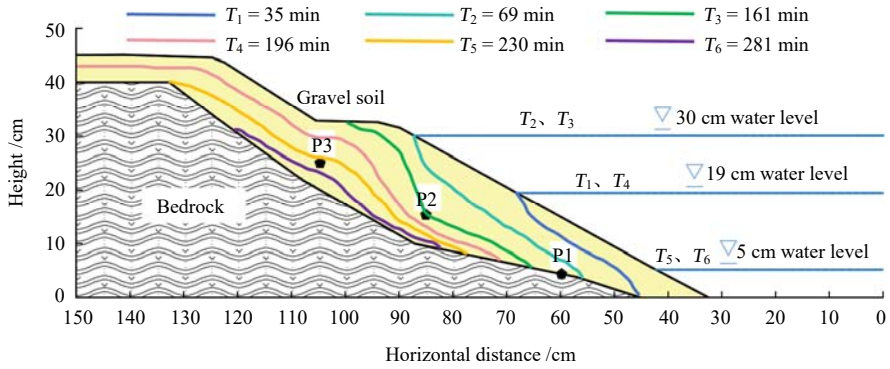


Fig. 14 Migration and evolution process of wetting front under condition 2

wetting front in the slope of the non-submerged section are consistent with condition 1. This is mainly due to the reservoir water in the reservoir area of the pressure exerted on the slope body increases the depth of reservoir water infiltration, only the existence of rainfall, due to the slope surface has been partially saturated, most of the rainfall will be in the formation of runoff on the surface of the slope, coupled with the infiltration of rainfall is also weaker than the reservoir water, so the size of the subsequent downward migration of the moist peak will be a significant decrease. The final wetting front is still characterized by a “hump type”, but its downward peak depth increases by about 7 cm compared with condition 1, and the trend of monitoring data within its range is also larger than that of condition 1.

Ultimately, condition 1 migrated about 90% of the total area of the slope flanks. In contrast, condition 2 accounted for approximately 97%, of which approximately 53% was in the presence of water level fluctuations only. This shows that the depth of the wetting front mainly depends on the mode and time of infiltration, while its final form is mainly controlled by the slope shape. In addition, the magnitude of the migration rate is related to the gravity characteristics of the seepage field, the slope gradient, and the location and characteristics of the dominant infiltration gullies. The overall downward migration rate under the two working conditions is characterized by fast to slow, the front of the slope is larger than the back of the slope, and the concave part of the slope is larger than the protruding part[42].

When the reservoir water level rises to the elevation of the monitoring point, the response of the pore water pressure is delayed due to the time difference of the reservoir water infiltration. The lag time is the time difference between the reservoir water level reaching the monitoring point elevation and its pore water pressure response. The larger the time difference is, the more significant the lag effect is. Figure 9(b) shows that the values of P1 and P2 increase slowly when the water level is low, but then accelerate with the rise of water level. Combined with the reservoir water scheduling law and the law of linear seepage, it can be seen that the height of the water level is inversely proportional to the rate of water level rise and fall, and the rate of water level rise and fall is proportional to the difference between the head inside and outside the slope. From this, we know that the water level fluctuation rate is proportional to the pore water pressure hysteresis effect when the water level rises.

Under the same conditions, compared with the soil bank slope, the bank slope with sand layer is more sensitive to the fluctuation of reservoir water because of the higher permeability coefficient of the internal sand layer. The water level fluctuation rate is more proportional to the permeability rate of the reservoir water in the layer, and the permeability rate of the reservoir water is inversely proportional to the hysteresis effect of pore water pressure. Therefore, the water level fluctuation rate of the bank slope with sand layer is inversely proportional to the hysteresis effect of pore water pressure when the water level rises. This conclusion is contrary to this study[4].

In addition, analyzing the pore water data at each monitoring point under the two conditions, it was found that the change value of pore water pressure in the shallow layer of the bank slope was larger than that in the deep layer at the beginning of the water level fluctuation or rainfall, but eventually the change magnitude of the pore water pressure in the deep layer of the slope body was larger, and this conclusion was verified by comparing the numerical curves of P2 and P3 in conditions 1 and 2 and by the analysis of the Mann-Whitney U in the previous section, and it is basically in line with the findings of many scholars[43−44].

Figure 9(b) illustrates the variation features of soil pressure. Soil pressure increases slowly with reservoir water volume, spikes sharply when water reaches the upper slope surface at the monitoring point, and then rises slowly as water infiltrates. It experiences another sharp increase upon reaching the monitoring point and stabilizes when soil is partially saturated. The water level drops, the reservoir water volume decreases, the soil on the slope surface of the hydro-fluctuation belt is lost, the weight of the overlying soil of #1 and #2 decreases, and the soil pressure decreases. Especially when the water level drops to the upper slope of the monitoring point, the earth pressure will show a sharp downward trend. If the subsequent erosion gully undercuts to the point where the monitoring point is buried, then the soil pressure will drop off a cliff.

When the water level rises, a seepage pressure forms on the slope surface due to differences in internal and external water levels. This pressure enhances the slope's resistance to sliding and limits plastic deformation, leading to only minor visible signs of deformation. It is concluded that reservoir impoundment stabilizes bank slopes within a certain range of water level rise[45−46]. When the water level drops, the reservoir water stored in the slope is discharged when the rainfall recharge is smaller than the seepage discharge, and dynamic water pressure is generated, resulting in pipe surge and submerged erosion, causing fine granular materials in the slope to flow out from the slope surface along the seepage gully, and accumulating at the foot of the slope to form a shallow bank, resulting in turbidity of the reservoir water and causing localized damages, which is especially significant in the late stage of the drop of the water level. Thus, a faster drop rate within a certain range leads to stronger seepage effects, longer slope infiltration times, and more severe surface deformation[47].

In addition, the test process also found that the main erosion gully of the slope under the two conditions are developed on both sides of the slope, which may be due to the rainfall nozzle for the full-circle nozzle, spraying a larger range, part of the sprayed water is concentrated in the inner wall of the glass box and downstream, resulting in increased erosion of the lower slope, resulting in the slope runoff is easy to concentrate on both sides of the slope, the erosion intensity increases, and the gully is more likely to be formed. It may also be due to the lower compaction or surface unevenness on both sides of the slope, thus the follow-up study needs to pay attention to the selection of rainfall spray nozzles and the uniformity of the model slope system operation.

Due to significant deformation characteristics of the slope under this working condition, which resemble actual local conditions, we integrate the deformation evolution of the model slope surface with mechanical theory. The mechanisms behind deformation and fragmentation of the gravel soil bank slope under rainfall and water level coupling are summarized as follows (see Fig. 15):

①Slope expansion softening stage. At this stage, the slope's surface soil absorbs water and expands due to its swelling characteristics, causing initial expansion when reservoir water immerses it. However, this effect diminishes as the water infiltrates gradually. At the same time, the slope surface soil layer is locally saturated due to reservoir water infiltration, and the soil is water-sensitive, thus leading to a reduction in its strength parameters and a significant hydrotropic weakening effect. (Fig. 15(b)).

②Slope softening settlement stage. At this stage, the water-immersed soil of the reservoir is compacted due to the self-weight and seepage pressure of the reservoir water, the internal voids are filled and compressed, and the slope surface appears settlement. The soil is saturated from reservoir water infiltration, leading to reduced self-weight due to buoyancy. This causes decreased shear strength and diminished anti-sliding force in the sliding zone, significantly weakening slope stability (Fig. 15(c)).

③Erosion rill development stage. At this stage, due to the dual effects of reservoir water decline drag and slope runoff erosion, combined with the decrease of soil strength due to water-induced weakening, the surface of the water-level-fluctuating zone formed beaded small erosion caves at the initial stage of water level decline, and formed discontinuous erosion rills under subsequent rainfall erosion (Fig. 15(d)).

④Erosion rill expansion stage. In this stage, the scale of erosion rill increases significantly under the combined effect of rainfall erosion and pipe-surge type infiltration deformation and submerged erosion. In addition, the rapid decline rate of reservoir water, coupled with its

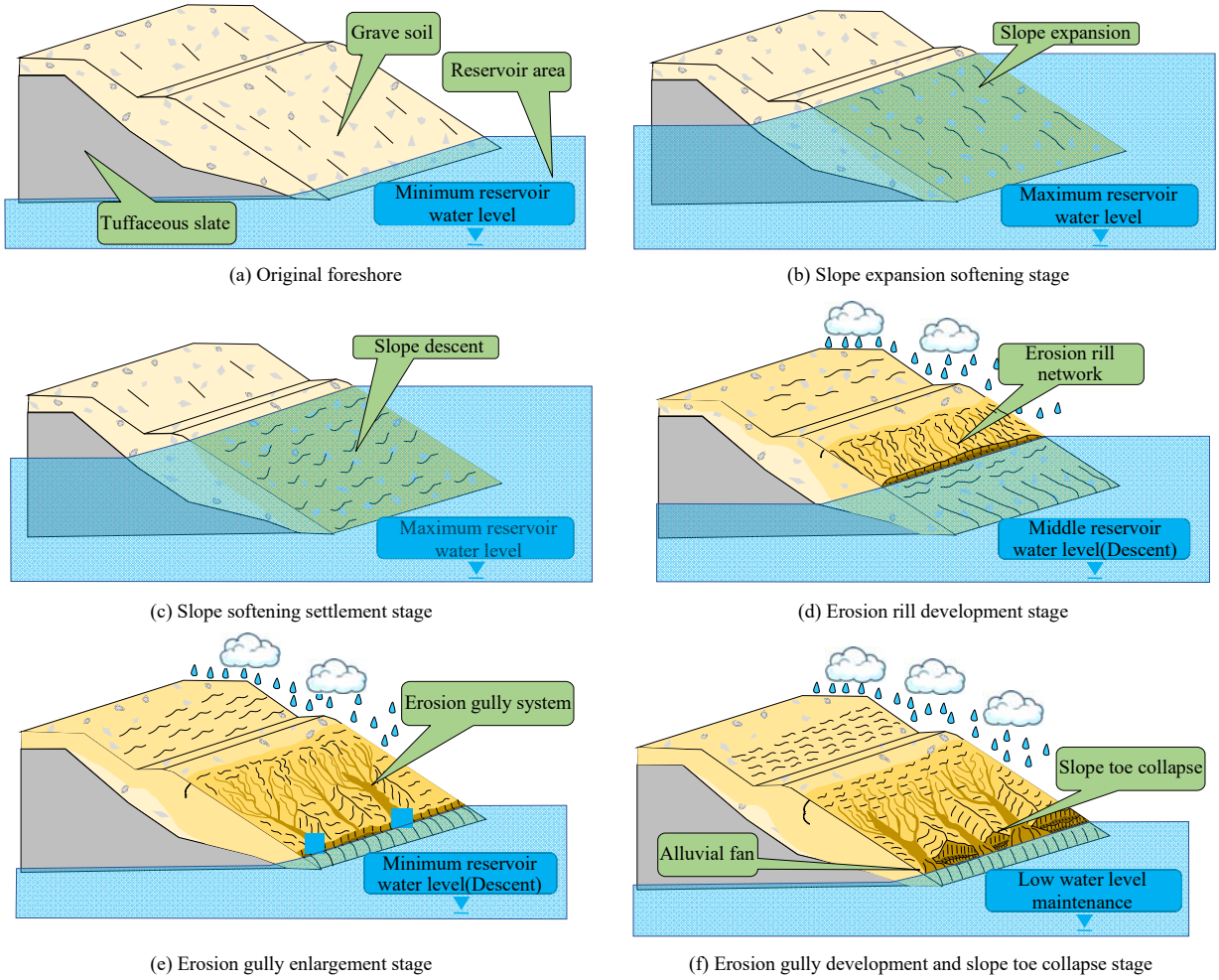


Fig. 15 Evolution stage of bank slope deformation

strong carrying capacity and significant seepage effects in the later stages, will further intensify slope erosion and lead to the formation of erosion gully (Fig. 15(e)).

⑤Erosion gully development and slope toe collapse stage. In this stage, runoff on the slope is intensified by the erosion gully convergence, enhancing both side and downward erosion. In addition, there are a large number of erosion rills in the hydro-fluctuation belt, which are easy to penetrate, so the scale of erosion gully expansion is significant. Furthermore, prolonged soaking of the slope toe by reservoir water weakens its strength. This reduction in uplift force decreases the anti-sliding force, making the slope toe more susceptible to collapse under ongoing runoff erosion (Fig. 15(f)).

To summarize, for this working condition of the water level drop section, the deformation characteristics of the fallout zone when the water level drops are varied, and the deformation damage mechanism is unique. In this stage, total stress on the bank slope rises, effective stress falls, and slope deformation becomes significant. The pore water pressure in the fluctuating zone decreases due to groundwater discharge, causing stress redistribution. This causes soil consolidation settlement and accelerates slope surface deformation and failure. At the same time, rainfall also exerts dynamic scouring load on the slope, weakens the mechanical characteristics of the slope, and superimposes the seepage force, resulting in a decrease in the anti-sliding force of the slope foot and a prominent slump phenomenon. As the erosion rill gradually transforms into an erosion gully, the leading edge of the slope undergoes significant erosion and scouring. Furthermore, the stability of the slope toe diminishes due to prolonged immersion and softening caused by reservoir water. This process ultimately causes localized collapse at the slope toe, marked by multi-stage sliding surface traction failure (Fig. 10).

6 Conclusion

Based on similarity theory and natural materials, physical model tests were conducted to examine the relationship between mechanical values such as pore water pressure in bank slopes and slope deformation and failure during rainfall and fluctuating water levels. The mechanisms of slope deformation, failure, and the characteristics of wetting front migration were elucidated. The main conclusions are as follows:

(1) Under the two conditions, the wetting front on the side of the slope was shallow in the middle and deep on the side, but the wetting front moved downward more

obviously under the coupling of rainfall and water level. The shape of the wetting front is mainly determined by the slope shape, the migration depth is controlled by the infiltration mode and time, and the migration rate is significantly affected by the characteristics of the seepage field and the slope.

(2) Under the effect of rainfall, the soil pressure and pore water pressure at each monitoring point show the trend of slow increase-surge-stable fluctuation, while under the coupled condition of water level fluctuation and rainfall, there is a slow decrease in the two values after the surge due to the drop of water level. Under the two conditions, the soil pressure curve changes gently and the pore water pressure changes with a lag, while the fluctuation amplitude of soil pressure and pore water pressure in the deeper layer of the slope is larger than that in the shallower layer under the saturated state.

(3) Under the rainfall condition, the strength of the soil body is weakened, the stability of the slope body is reduced, and the slope surface is characterized by the deformation and damage of erosion gullies and local landslides. Under coupled conditions, the water level rises within a certain range, the slope stability is enhanced by infiltration pressure; when the water level falls, rainfall erosion and softening by reservoir water immersion lead to the deterioration of the stability of the ablation zone, and the erosion gully is widely developed. Eventually, the amount of slope erosion under the coupled action of rainfall and water level is about twice as much as that of single rainfall, and multi-stage sliding surface progressive slope foot collapse phenomenon occurs in both conditions.

(4) The deformation and damage mechanism of gravel soil bank slopes under the coupling of rainfall and water level are summarized as follows: the expansion and softening stage of the slope surface at the beginning of the water level rise; the softening and settling stage of the slope surface at the time of stabilization of the high water level; the development stage of the erosion rill of the fall zone at the middle stage of the water level decline; the development stage of the erosion gully at the later stage of the water level decline; and the collapse stage of the foot of the slope at the time of stabilization of the low water level.

(5) According to the test results, in order to prevent further deformation and damage of the bank slope, it is recommended to take the following measures: for the development of erosion gullies and seepage in the slope, construct drainage facilities; for the existing large-scale collapse of the bank slope, strengthen the monitoring and early warning and slope protection.

For the gravel soil bank slopes with high gradient, thick cover layer, high rainfall in the rainy season and rapid fluctuation of water level at the foot of the slopes, which have not yet experienced large-scale deformation, but still have the possibility of instability due to the gradual evolution of foot of the slopes collapsing. The above conclusions can provide references to the study of deformation and damage mechanism as well as the formulation of preventive and curative measures.

References

[1] MIAO Fa-sheng, WU Yi-ping, XIE Yuan-hua, et al. Centrifugal test on retrogressive landslide influenced by rising and falling reservoir water level[J]. Rock and Soil Mechanics, 2018, 39(2): 605−613.

[2] WANG Zhi-wang, YANG Jian, ZHANG Bao-Jun, et al. Study on stability of landside of reservoir area[J]. Rock and Soil Mechanics, 2004, 25(11): 1837−1840.

[3] JIANG Qiang-qiang, JIAO Yu-yong, SONG Liang, et al. Experimental study on reservoir landslide under rainfall and water-level fluctuation[J]. Rock and Soil Mechanics, 2019, 40(11): 4361−4370.

[4] ZHU Jun-hua, LÜ Qing, XIE Dian, et al. Physical model test on the deformation mechanism of reservoir bank slopes with sand layers under coupled hydro- mechanical conditions[J]. Frontiers in Earth Science, 2022, 10: 863370.

[5] XIE Jia-long, LI Yuan-yao, WANG Ning-tao, et al. Assessment of regional landslide hazard in Yunyang County considering the combined effect of reservoir water level and rainfall[J]. Journal of Yangtze River Scientific Research Institute, 2021, 38(12): 72-81, 90.

[6] JIAO Yu-yong, ZHANG Huan-qiang, TANG Hui-ming, et al. Simulating the process of reservoir-impoundment-induced landslide using the extended DDA method[J]. Engineering Geology, 2014, 182(PA): 37−48.

[7] GATTO L W, DOE III W W. Bank conditions and erosion along selected reservoirs[J]. Environmental Geology Water Sciences, 1987, 9(3): 143−154.

[8] KAFLE J, POKHREL P R, KHATTRI K B, et al. Landslide-generated tsunami and particle transport in mountain lakes and reservoirs[J]. Annals of Glaciology, 2016, 57(71): 232−244.

[9] SENGANI F, MULENGA F. Influence of rainfall intensity on the stability of unsaturated soil slope: case study of R523 road in Thulamela Municipality, Limpopo Province, South Africa[J]. Applied Sciences, 2020, 10(24): 8824.

[10] WANG Huan-ling, JIANG Zi-hua, XU Wei-ya, et al. Physical model test on deformation and failure mechanism of deposit landslide under gradient rainfall[J]. Bulletin of Engineering Geology the Environment, 2022, 81(1): 66.

[11] ZHANG Tian-dong, ZHANG Zi-zhao, CHEN Xu, et al. Destabilization mechanism of rainfall-induced loess landslides in the Kara Haisu Gully, Xinyuan County, Ili River Valley, China: physical simulation[J]. Water, 2023, 15(21): 3775.

[12] DAI F C, DENG J H, THAM L C, et al. A large landslide in Zigui County, Three Gorges area[J]. Canadian Geotechnical Journal, 2004, 41(6): 1233−1240.

[13] JIA G W, ZHAN L T, CHEN Y M, et al. Performance of a large-scale slope model subjected to rising and lowering water levels[J]. Engineering Geology, 2009, 106(1-2): 92−103.

[14] ZHAO Jian-jun, ZHANG Han-yue, YANG Chang-xing, et al. Experimental study of reservoir bank collapse in gravel soil under different slope gradients and water levels[J]. Natural Hazards, 2020, 102(1): 249−273.

[15] CHANG K T, HUANG H C. Three-dimensional analysis of a deep-seated landslide in central Taiwan[J]. Environmental Earth Sciences, 2015, 74(2): 1379−1390.

[16] XIAO Jie-fu, LI Yun-an, HU Yong, et al. Model tests on deformation characteristics of ancient bank landslide under water level fluctuation and rainfall[J]. Rock and Soil Mechanics, 2021, 42(2): 471−480.
[17] SUN Guan-hua, YANG Yong-tai, WEI Jiang, et al. Effects of an increase in reservoir drawdown rate on bank slope stability: a case study at the Three Gorges Reservoir, China[J]. Engineering Geology, 2017, 221: 61−69.
[18] HU Xin-li, TAN Fu-lin, TANG Hui-ming, et al. In-situ monitoring platform and preliminary analysis of monitoring data of Majiagou landslide with stabilizing piles[J]. Engineering Geology, 2017, 228: 323−336.
[19] XIA Ming, REN Guang-ming, MA Xin-lei. Deformation and mechanism of landslide influenced by the effects of reservoir water and rainfall, Three Gorges, China[J]. Natural Hazards, 2013, 68(2): 467−482.
[20] WANG Biao, YI Qing-lin, NIU Yan, et al. Analysis of deformation response law of large cataclastic bedding rock landslide under dynamic action of groundwater[J]. Chinese Journal of Rock Mechanics and Engineering, 2023, 42(Suppl.2): 4140−4151.
[21] MIAO Fa-sheng, WU Yi-ping, LI Lin-wei, et al. Centrifuge model test on the retrogressive landslide subjected to reservoir water level fluctuation[J]. Engineering Geology, 2018, 245: 169−179.
[22] SANZ D E, OJEDA P, SANZ E, et al. Retrospective analysis of the Pico del Castillo de Vinuesa large historical landslide (Cordillera Iberica, Spain)[J]. Landslides, 2020, 17(12): 2837−2848.
[23] ALONSO E E, PINYOL N M. Numerical analysis of rapid drawdown: applications in real cases[J]. Water Science and Engineering, 2016, 9(3): 175−182.
[24] XIA Ming, REN Guang-ming, ZHU Shao-shuai, et al. Relationship between landslide stability and reservoir water level variation[J]. Bulletin of Engineering Geology and the Environment, 2015, 74(3): 909−917.
[25] ZHANG Shi-lin, LÜ Peng-fei, YANG Xing-guo, et al. Spatiotemporal distribution and failure mechanism analyses of reservoir landslides in the Dagangshan reservoir, south-west China[J]. Geomatics, Natural Hazards and Risk, 2018, 9(1): 791−815.
[26] JIAN Wen-xing, XU Qiang, YANG Hu-feng, et al. Mechanism and failure process of Qianjiangping landslide in the Three Gorges Reservoir, China[J]. Environmental Earth Sciences, 2014, 72(8): 2999−3013.
[27] PARONUZZI P, RIGO E, BOLLA A. Influence of filling–drawdown cycles of the Vajont reservoir on Mt. Toc slope stability[J]. Geomorphology, 2013, 191: 75−93.
[28] IVERSON R M. Scaling and design of landslide and debris-flow experiments[J]. Geomorphology, 2015, 244: 9−20.
[29] LI Chi, YAO De, WANG Zhong, et al. Model test on rainfall-induced loess–mudstone interfacial landslides in Qingshuihe, China[J]. Environmental Earth sciences, 2016, 75(9): 1−18.
[30] JIANG Zi-hua, WANG Huan-ling, XIE Wei-zhou. Deformation mechanism of deposit landslide induced by fluctuations of reservoir water level based on physical model tests[J]. Environmental Earth Sciences, 2021, 80(11): 411−413.
[31] TOHARI A, NISHIGAKI M, KOMATSU M. Laboratory rainfall-induced slope failure with moisture content measurement[J]. Journal of Geotechnical and Geoenvironmental Engineering, 2007, 133(5): 575−587.
[32] LUO Xian-qi, LIU De-fu, WU Jian, et al. Model test study on landslide under rainfall and reservoir water fluctuation[J]. Chinese Journal of Rock Mechanics and Engineering, 2005, 24(14): 2476−2483.
[33] LI Zhuo, HE Yong-jun, SHENG Jin-bao, et al. Landslide model for slope of reservoir bank under combined effects of rainfall and reservoir water level[J]. Chinese Journal of Geotechnical Engineering, 2017, 39(3): 452−489.
[34] DAI Zhen-wei, ZHANG Yan-jun, ZHANG Chen-yang, et al. Interpreting the influence of reservoir water level fluctuation on the seepage and stability of an ancient landslide in the Three Gorges Reservoir area: a case study of the Outang landslide[J]. Geotechnical and Geological Engineering, 2022, 40(9): 4551−4561.
[35] HU Xin-li, HE Chun-can, ZHOU Chang, et al. Model test and numerical analysis on the deformation and stability of a landslide subjected to reservoir filling[J]. Geofluids, 2019, 2019(1): 5924580.
[36] WANG Hua. Study of deformation and failure mechanism of bridge foundation slope with physical simulation method[J]. Rock and Soil Mechanics, 2011, 32(7): 2034−2038.
[37] Ministry of Housing and Urban-Rural Development of People's Republic of China. GB/T50123 — 2019. Standard for geotechnical testing method[S]. Beijing: China Planning Press, 2019.
[38] HAMROUNI F, TRABELSI H, JAMEI M, et al. Numerical analysis of landslides caused by rainfall in a reduced physical slope model[J]. European Journal of Environmental and Civil Engineering, 2021, 25(8): 1449−1470.
[39] ZHAN Qing-hua, WANG Shi-mei, GUO Fei, et al. Early warning model and model test verification of rainfall-induced shallow landslide[J]. Bulletin of Engineering Geology and the Environment, 2022, 81(8): 318.
[40] IZUMI A, SAWADA Y, HORI T, et al. Centrifuge modelling of small earth dams subjected to the combined effects of rainfall and earthquakes[J]. Soil Dynamics and Earthquake Engineering, 2021, 151: 106−963
[41] ZHU Yuan-jia, HE Na, ZHONG Wei, et al. Physical simulation study of deformation and failure accumulation layer slope caused by intermittent rainfall[J]. Rock and Soil Mechanics, 2020, 41(12): 4035−4044.
[42] CHENG Qian, LI Ya-jun, VARDAN P J, et al. Temporal stability and risk analysis of soil slopes subject to rainfall: The influence of heterogeneity[J]. Engineering Geology, 2025, 347: 107895.
[43] ZHAN Qing-hua, WANG Shi-mei, TAN Yun-zhi, et al. Experimental study on the influence of rainfall and reservoir water on landslide behavior[J]. Journal of Changjiang River Scientific Research Institute, 2013, 30(11): 32−38.
[44] ZHAN Qing-hua, WANG Shi-mei, ZHAO Dai-peng. Experimental study on the impact of reservoir water rise on the stability of landslides with weak interlayers[J]. Journal of Changjiang River Scientific Research Institute, 2016, 33(2): 86−90.
[45] JI Feng, LIU Chang-jiang, ZHOU Hui-xing, et al. Identifying the influences of geological factors on reservoir bank collapse by a model test[J]. Bulletin of Engineering Geology and the Environment, 2018, 77(1): 127−139.
[46] PENG Shi-xiong. State-of-art art of bank collapse predicting of reservoir and a balanced alluvial accumulation approach[J]. Chinese Journal of Rock Mechanics and Engineering, 2014, 33(11): 2332−2340.
[47] WANG Ning-tao, LIU Lei, SHI Ting-ting, et al. Study of the impact of reservoir water level decline on the stability treated landslide on reservoir bank[J]. Alexandria Engineering Journal, 2023, 65: 481−492.